(MOD),[16] it is not surprising to find d_{CuC} and d_{CuO} much shorter than those obtained by the other calculations. This is due to the enlarged basis set extention error (BSSE),[19] which tends to shorten the bonds formed during complexation.

The results of MP2 and CPF calculations are in good agreement. Coordination of one CO ligand to the copper atom of CuCl changes neither the length of the CO bond nor that of the CuCl bond very much. On the other hand, there is a pronounced difference in the copper-ligand distance between the two complexes; coordination via the C atom brings the ligand CO more than 10 pm closer to the central atom.

The calculated distances in Cu(CO)Cl are close to the equivalent values in copper(I) carbonyl complexes obtained with X-ray methods. To give an example, for the recently characterized solid Cu(CO)Cl,[3] the CO and CuC distances are 111.2 and 185.6 pm, respectively. Because of the polymeric character of this compound, the CuCl bond is longer (d_{CuCl} = 237.0 pm) than in the monomeric species.

From the differences in total energy between isolated CuCl and CO on one side and Cu(CO)Cl and Cu(OC)Cl, respectively, on the other side, the energies for the reactions of complexation have been determined by the CPF method (values obtained by MP2 calculations are given in parentheses):

$$CuCl + CO \rightarrow Cu(CO)Cl + 155.2 \text{ kJ mol}^{-1} (195.6 \text{ kJ mol}^{-1})$$

$$CuCl + CO \rightarrow Cu(OC)Cl + 49.3 \text{ kJ mol}^{-1} (53.3 \text{ kJ mol}^{-1})$$

As expected, coordination of CO with the C atom is the favored process. The energy for this reaction is of the magnitude of the energy for the first coordination of a CO molecule to a nickel atom, which is found to be approximately 140 kJ mol^{-1}.[20]

Frequencies and intensities within the harmonic approximation could only be computed on the MOD level. The results are presented in Table V. Obviously, the best agreement between experiment and calculation is obtained for Cu(CO)Cl. In accordance with the experimental IR spectra, the most intense band is calculated for the CO absorption. It is shifted to higher wavenumbers compared to that of the isolated molecule CO (observed shift +19 cm^{-1}; calculated shift +11 cm^{-1}). The only other absorption ($\nu_{ClCu/CuCO}$) that is predicted to be observable for Cu(CO)Cl is about 10 times weaker in intensity than the corresponding CO band. Compared to the frequency of isolated CuCl, $\nu_{ClCu/CuCO}$ is calculated to be shifted to lower wavenumbers.

According to our calculations for the molecule Cu(OC)Cl, one would have expected a red-shifted CO absorption compared to that of isolated CO. A second band expected for this molecule is calculated to be 3 times weaker in intensity than the first one, which is blue-shifted with respect to that of isolated CuCl. Both predictions are in contrast to the experimental observations. Therefore, only the calculated spectra of Cu(CO)Cl provide an accurate fit with the experimental findings for both intensities and frequencies.

An analysis of the CPF wave function shows that bonding between copper and carbon in Cu(CO)Cl mainly is of the σ type. A smaller amount of π-back-bonding from d orbitals located at Cu into the π^* LUMO of CO is detectable, however. In terms of a Roby-Davidson population analysis,[21] the σ shared electron number (σ-SEN) for the CuC bond is 1.4 whereas the π-SEN is 0.1 only. This point of view of CO as a σ-donor and a weak π-acceptor is further supported by the results of a Mulliken population analysis,[22] which shows a transfer of electrons from CO to Cu in the σ-space of about 0.4 e; π-back-bonding amounts to about 0.2 e.

Conclusion

Experimental as well as theoretical results confirm the assignments to a linear molecule Cu(CO)Cl formed under cryogenic matrix isolation conditions. The CuC bond is mainly formed by electron transfer out of the σ HOMO of the ligand into d_σ orbitals of the copper atom; there is evidence for some π-back-bonding from Cu to C, which plays a minor role.

Acknowledgment. This work was supported by the Deutsche Forschungsgemeinschaft. We thank the Leibniz Rechenzentrum der Bayerischen Akademie der Wissenschaften and RZ Karlsruhe for providing computational facilities. M.R.B. was supported by a Graduiertenstipendium from the state of Baden-Württemberg.

(19) Lin, B.; McLean, A. D. *J. Chem. Phys.* **1973**, *59*, 4557; **1989**, *91*, 2348.
(20) Stevens, A. E.; Feigerle, C. S.; Lineberger, W. C. *J. Am. Chem. Soc.* **1982**, *104*, 5026.
(21) Davidson, E. R. *J. Chem. Phys.* **1967**, *46*, 3320. Roby, K. R. *Mol. Phys.* **1974**, *27*, 81. Heinzmann, R.; Ahlrichs, R. *Theor. Chim. Acta* **1976**, *42*, 33.
(22) Mulliken, R. S. *J. Chem. Phys.* **1955**, *23*, 1833.
(23) Huzinaga, S. Approximate Atomic Functions I+II. The University of Alberta, 1971.
(24) Dolg, M.; Wedig, U.; Stoll, H.; Preuss, H. *J. Chem. Phys.* **1986**, *86*, 866.

Contribution from the Department of Chemistry and Biochemistry, University of Notre Dame, Notre Dame, Indiana 46556, and Department of Chemistry and Biochemistry, University of Delaware, Newark, Delaware 19716

Boron in New Environments. Structure and Reaction Properties of Discrete, Mixed-Metal, Hexanuclear Borides

A. K. Bandyopadhyay,[†] Rajesh Khattar,[†] J. Puga,[†] T. P. Fehlner,*[,†] and A. L. Rheingold*[,‡]

Received May 3, 1991

The preparation and characterization of two discrete, mixed-metal, hexanuclear transition-metal borides, *trans*-$[Fe_4Rh_2(CO)_{16}B]^-$ and *mer*-$H_2Fe_3Rh_3(CO)_{15}B$, are described. The former is prepared from the boride precursor, $[HFe_4(CO)_{12}BH]^-$, by a cluster expansion reaction with $[Rh(CO)_2Cl]_2$, while the latter forms spontaneously on protonation of *trans*-$[Fe_4Rh_2(CO)_{16}B]^-$. Both have been characterized spectroscopically and crystallographically. However, *mer*-$H_2Fe_3Rh_3(CO)_{15}B$ is severely disordered in the solid state, prohibiting definition of the interatomic distances of this species. Both compounds exhibit an octahedral metal framework with a centered, six-coordinate boron atom. The IR absorptions associated with the interstitial boron atom have been identified in both. The formation of *trans*-$[Fe_4Rh_2(CO)_{16}B]^-$ is preceded by the formation of *cis*-$[Fe_4Rh_2(CO)_{16}B]^-$, and the mechanism of the isomerization process has been investigated. Evidence is presented for a Lewis base promoted process in which rapid, reversible base coordination precedes isomerization as well as ligand substitution. The isomerization process is more rapid than ligand substitution for PMe_2Ph as the entering ligand.

The boron atom in mononuclear compounds is usually found with three or four nearest neighbors. This is consistent with the atomic structure of boron, the concept of a two-center-two-electron bond, and Lewis acid-base chemistry.[1] However, the fact that

[†] University of Notre Dame.
[‡] University of Delaware.

(1) Greenwood, N. N.; Earnshaw, A. *Chemistry of the Elements*; Pergamon: Oxford, U.K., 1984.

0020-1669/92/1331-0465$03.00/0

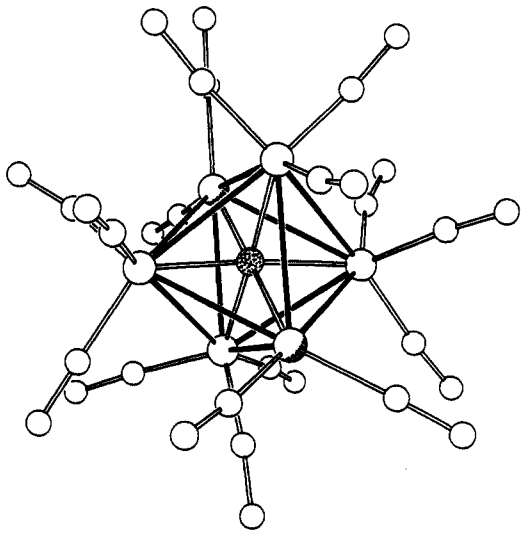

Figure 1. Molecular structure of *trans*-$[Fe_4Rh_2(CO)_{16}B][PPN]$.[18] Shaded atoms are Rh, unshaded atoms are Fe, and the stippled atom is B.

boron possesses one more valence orbital than valence electrons generates a proclivity for multicenter bonding.[2] The most spectacular expression of this tendency is the richness of the deltahedral cluster structures exhibited by the polyboranes and related compounds.[3] In these species, a given boron can be within bonding distance of as many as six nearest-neighbor atoms. Although such complex bonding situations are hardly restricted to the element boron,[4] its tendency to adapt to the environment presented gives the chemistry of this element added zest. Indeed, the unusual bonding environments in which one can place a boron atom are not yet exhausted[5] and with transition metals the scope of possibilities is still being revealed.[6]

One unusual bonding environment of boron is that in which the boron atom is found in an "interstitial" hole in a closed, discrete transition-metal cluster.[7] In view of the above emphasis placed on the versatility of the bonding capabilities of boron and the fact that the chemistry of solid-state borides, with stoichiometries ranging from metal-rich to boron-rich, is vast in compound types and varied in structural modes,[8-14] the depiction of such a bonding environment as unusual requires comment. A variety of other main-group elements (groups 1, 14,[15] 15,[16] and 16[17]) have already been characterized in such environments. Thus, boron is unusual in that it was only until recently that definitive examples of such bonding were reported. Our group,[18] as well as three others,[19-21] have now communicated the isolation and characterization of discrete compounds containing boron atoms completely encapsulated by a metal framework. The most recent example is particularly interesting. The solution chemistry of solid phases containing boron atom centered zirconium clusters has been described and the discrete boride cluster structurally characterized along with analogues containing four other different interstitial atoms.[21] In the following, we describe in more detail the geometric structure as well as some of the spectroscopic properties and reaction chemistry of the discrete borides we have synthesized.

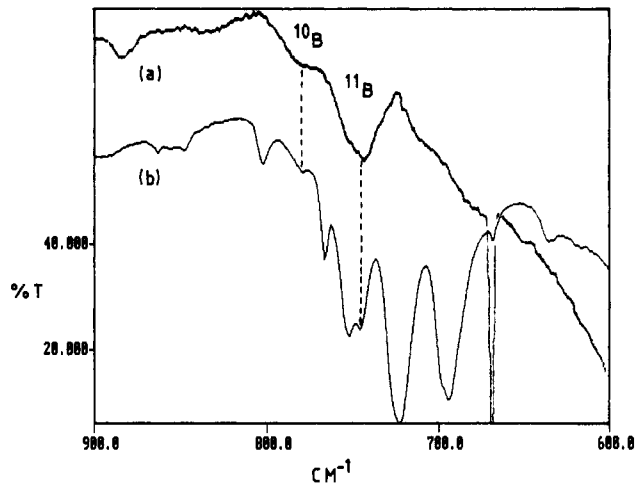

Figure 2. IR spectra of (a) *trans*-$[Fe_4Rh_2(CO)_{16}B][n\text{-}Bu_4N]$ and (b) *trans*-$[Fe_4Rh_2(CO)_{16}B][PPN]$ in Nujol mull at room temperature. Spectrum a is a difference spectrum, i.e., (sample + Nujol) − (Nujol).

Results and Discussion

The ferraborane $[HFe_3(CO)_9BH_3]^-$ undergoes a clean cluster-building reaction with $Fe_2(CO)_9$ to yield $[HFe_4(CO)_{12}BH]^-$.[22] However, further reaction of the tetranuclear cluster with either $Fe_2(CO)_9$ or a variety of other potential metal fragment sources has led thus far to loss of born from solution species (as monitored by ^{11}B NMR spectroscopy) and precipitation of uncharacterized solids. With one metal fragment source, $[Rh(CO)_2Cl]_2$, $[HFe_4(CO)_{12}BH]^-$ undergoes a complex, but facile, cluster-building reaction to initially yield the boride *cis*-$[Fe_4Rh_2(CO)_{16}B]^-$, which rearranges on standing to give *trans*-$[Fe_4Rh_2(CO)_{16}B]^-$ (Figure 1).[23] The structure has been presented in the initial communication.[18] Briefly, the latter anion has D_{2d} symmetry and consists of a distorted octahedral core of metal atoms, each with external CO ligands, encapsulating a single boron atom. The Rh atoms are trans to one another in a structure that maximizes the number of heterometallic bonds. Of particular note is the narrow, very low field triplet observed in the ^{11}B NMR spectrum which is

(2) Lipscomb, W. N. *Boron Hydrides*; Benjamin: New York, 1963.
(3) Wade, K. *Electron Deficient Compounds*; Nelson: London, 1971.
(4) Fehlner, T. P. *Comments Inorg. Chem.* **1988**, *7*, 307.
(5) Fehlner, T. P. In *Advances in Boron and the Boranes*; Liebman, J. F., Greenberg, A., Williams, R. E., Eds.; VCH: New York, 1988; p 265.
(6) Fehlner, T. P. *New J. Chem.* **1988**, *12*, 307. Housecroft, C. E. *Polyhedron* **1987**, *6*, 1935. Grimes, R. N., Ed. *Metal Interactions with Boron Clusters*; Plenum: New York, 1982. Housecroft, C. E.; Fehlner, T. P. *Adv. Organomet. Chem.* **1982**, *21*, 57. Kennedy, J. D. *Prog. Inorg. Chem.* **1984**, *32*, 519; **1984**, *34*, 211.
(7) Evidence for the existence of a hexacobalt boride has been presented: Schmid, G.; Bätzel, V.; Etzrodt, G.; Pfeil, R. *J. Organomet. Chem.* **1975**, *86*, 257.
(8) Greenwood, N. N.; Parish, R. V.; Thornton, P. *Q. Rev., Chem. Soc.* **1966**, *20*, 441.
(9) Matkovich, V. I., Ed. *Boron and Refractory Borides*; Springer-Verlag: Berlin, 1977.
(10) Post, B. In *Boron, Metallo-Boron Compounds and Boranes*; Adams, R. M., Ed.; Interscience: New York, 1964; p 301.
(11) Aronsson, B.; Lundström, T.; Rundqvist, S. *Borides, Silicides and Phosphides*; Methuen: London, 1965.
(12) Lundström, T. In *Boron and Refractory Borides*; Matkovich, V. I., Ed.; Springer-Verlag: Berlin, 1977; p 351.
(13) Thompson, R. *Prog. Boron Chem.* **1970**, *2*, 173.
(14) Lipscomb, W. N. *J. Less-Common Met.* **1981**, *82*, 1.
(15) Bradley, J. S. *Adv. Organomet. Chem.* **1983**, *22*, 1 and references therein. Eady, C. R.; Jackson, P. F.; Johnson, B. F. G.; Lewis, J.; Malatesta, M. C.; McPartlin, J.; Nelson, W. J. H. *J. Chem. Soc., Dalton Trans.* **1980**, 383. Mackay, K. M.; Nicholson, B. K.; Robinson, W. T.; Sims, A. W. *J. Chem. Soc., Chem. Commun.* **1984**, 1276.
(16) Ciani, G.; Martinengo, S. *J. Organomet. Chem.* **1986**, *306*, C49. Martinengo, S.; Ciani, G.; Sironi, A.; Heaton, B. T.; Mason, J. *J. Am. Chem. Soc.* **1979**, *101*, 7905. Bonfichi, R.; Ciani, G.; Sironi, A.; Martinengo, S. *J. Chem. Soc., Dalton Trans.* **1983**, 253. Vidal, J. L. *Inorg. Chem.* **1981**, *20*, 243. Vidal, J. L.; Troup, J. M. *J. Organomet. Chem.* **1981**, *213*, 351.
(17) Colbran, S. B.; Lahoz, F. J.; Raithby, P. R.; Lewis, J.; Johnson, B. F. G.; Cardin, C. J. *J. Chem. Soc., Dalton Trans.* **1988**, 173. Ciani, G.; Graslaschelli, L.; Sironi, A. *J. Chem. Soc., Chem. Commun.* **1981**, 563. Vidal, J. L.; Fiato, R. A.; Cosby, L. A.; Pruett, R. L. *Inorg. Chem.* **1978**, *17*, 2574.
(18) Khattar, R.; Puga, J.; Fehlner, T. P.; Rheingold, A. L. *J. Am. Chem. Soc.* **1989**, *111*, 1877.
(19) Harpp, K. S.; Housecroft, C. E.; Rheingold, A. L.; Shongwe, M. S. *J. Chem. Soc., Chem. Commun.* **1988**, 965.
(20) Hong, F. E.; Coffy, T. J.; McCarthy, D. A.; Shore, S. G. *Inorg. Chem.* **1989**, *28*, 3284.
(21) Rogel, F.; Corbett, J. D. *J. Am. Chem. Soc.* **1990**, *112*, 8198.
(22) Housecroft, C. E.; Fehlner, T. P. *Organometallics* **1986**, *5*, 379.
(23) Bandyopadhyay, A. K.; Khattar, R.; Fehlner, T. P. *Inorg. Chem.* **1989**, *28*, 4436.

characteristic of the presence of a boron atom in a highly symmetrical electronic environment directly bonded to many metal atoms, two of which are rhodium.[24] The cluster core is sheathed in carbonyl ligands such that there are two $Rh(CO)_2$ groups staggered with respect to each other and four $Fe(CO)_3$ groups with each pair of trans groups eclipsed with respect to each other. Consistent with the solution infrared studies, all the CO ligands are terminal although the CO ligands lying above the long Rh–Fe edges might be judged semibridging. Although the first-formed boride could not be isolated and crystallographically characterized, the ^{11}B NMR parameters are sufficiently distinctive to define it as the cis isomer. In the following, some more detailed structural studies of the isomerization and protonation reactions are described.

Vibrational Studies. One of the characteristic features of the infrared spectra of metal clusters containing interstitial main-group atoms are the relatively intense absorptions exhibited in the energy range 700–900 cm^{-1}.[25] These have been assigned to the metal–main-group interstitial atom stretching modes and often are found to reflect the symmetry[26] and force field environment of the interstitial atom.[27] However, it has been found that differences in solid-state site symmetry can also affect the complexity of the spectrum observed particularly at low temperatures.[28]

The appropriate region of the vibrational spectrum of $[Fe_4Rh_2(CO)_{16}B]^-$ with two different counterions is shown in Figure 2. Bands associated with the $[PPN]^+$ counterion partially obscure the region of interest, but two bands, clearly evident in the spectrum of the $[Bu_4N]^+$ salt, are also present as shoulders in the spectrum of the $[PPN]^+$ salt. The asymmetrical band with a maximum at 743 cm^{-1} is assigned to the modes associated with the interstitial ^{11}B atom whereas the weaker band at 781 cm^{-1} is assigned to the ^{10}B atom in the isotopomer. (The natural abundance of ^{10}B is 20%, and the calculated frequency of this band is 780.3 cm^{-1}.) The shoulder on the 743-cm^{-1} band at $\approx$753 cm^{-1}, clearly present in the spectrum of the $[Bu_4N]^+$ salt, reflects a site symmetry lower than O_h. Note that the number of bands observed often reflects the core symmetry rather than the molecular symmetry.[25] In the case of *trans*-$[Fe_4Rh_2(CO)_{16}B]^-$, however, because of the fold in the Fe_4 fragment, both the Fe_4Rh_2 core and the cluster itself have D_{2d} symmetry. A simple model for the interstitial modes results from the consideration of the M_6B metal cluster as a rigid framework of octahedral geometry and the vibrational motion of the interstitial atom as that of a three-dimensional, harmonic oscillator. For the Fe_4Rh_2B system, this model suggests that two vibrational frequencies should be observed, with the lower frequency mode being doubly degenerate. Hence, we associate the 743-cm^{-1} band maximum with the FeB force constant and the 753-cm^{-1} shoulder with the RhB force constant. In turn, this suggests that, despite the greater Rh–B distance (d(Fe–B) = 1.94 Å, d(Rh–B = 2.03 Å), the interaction of the boron atom with the rhodium atoms is somewhat stronger than that with the iron atoms.

Particularly relevant for comparison with these observations is the vibrational study of the set of octahedral carbido clusters including $[Fe_6(CO)_{16}C]^{2-}$.[29] This carbido anion has C_s symmetry, and as expected, three overlapping bands are observed with maxima at 818, 790, and 776 cm^{-1}. For interstitial carbides, it has been found that the greater the MC distance, the smaller the MC force constant.[30] Thus, the smaller the interstitial hole, the higher the vibrational frequency. The smallest stretching frequency of the $[Fe_6(CO)_{16}C]^{2-}$ cluster is 23 cm^{-1} greater than the highest frequency of the $[Fe_4Rh_2(CO)_{16}B]^-$ cluster. In accord with the trends found for the series of carbido clusters, the interstitial hole in the borido cluster is significantly larger than that in the carbido cluster (d(Fe–C) = 1.89 Å). The perturbations caused by the presence of two Rh atoms in the boride cluster and the overall cluster charge difference appear small relative to the identity of the main-group atom.

Table I. Pseudo-First-Order Rate Constants for the Reaction

cis-$[Fe_4Rh_2(CO)_{12}(Y)_4B]^-$ + L → *trans*-$[Fe_4Rh_2(CO)_{12}(Y)_4B]^-$ + L

$[C]^+$	$(Y)_4$	k, min^{-1} × 10^3	solvent	T, K	L[a]
Na	$(CO)_4$	0.44	THF	273.0	–
Li	$(CO)_4$	4.4	THF	296.5	–
Na	$(CO)_4$	3.9	THF	296.5	–
K	$(CO)_4$	4.0	THF	296.5	–
Na	$(CO)_4$	21.2	THF	313.0	–
Na	$(CO)_4$	119.4	THF	328.0	–
Na	$(CO)_4$	18.2	Et_2O	296.5	–
Na	$(CO)_4$	11.3	glyme	296.5	–
Na	$(CO)_4$	13.6	glyme	296.5	excess $[Rh(CO)_2Cl]_2$
Na	$(CO)_4$	5.7[b]	THF	296.5	$NaHCO_3$
Na	$(CO)_4$	4.9[b]	THF	296.5	–
Na	$(CO)_4$	6.8	THF	296.5	NEt_3 (excess)
Na	$(CO)_4$	1.2[c]	THF	296.5	purge N_2
Na	$(CO)_4$	16.0[c]	THF	296.5	PMe_2Ph (0.025 M) purge N_2
Na	$(CO)_4$	1.5	THF	296.5	CO (5% in N_2)
Na	$(CO)_4$	4.6	THF	296.5	CO (15% in N_2)
Na	$(CO)_4$	6.0	THF	296.5	CO (20% in N_2)
Na	$(CO)_4$	7.2	THF	296.5	CO (25% in N_2)
Na	$(CO)_4$	10.0	THF	296.5	CO (35% in N_2)
Na	$(CO)_4$	13.8	THF	296.5	CO (50% in N_2)
Na	$(cod)_2$	5.5	THF	318.0	–

[a] The dash mark indicates no purge nor added reagents. [b] Measured in parallel. [c] Measured sequentially.

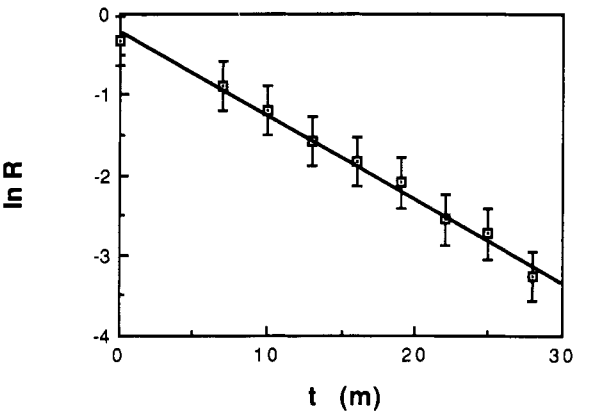

Figure 3. Plot of ln R vs t for the isomerization of *cis*-$[Fe_4Rh_2(CO)_{16}B]^-$ at 328 K, where $R = I_{\delta 205}/(I_{\delta 205} + I_{\delta 211})$, k = 0.104 min^{-1}, y = –0.219 – 0.104x, and R = 1.00. The bars represent the standard error of the data.

Reactivity: Isomerization. The fact that *trans*-$[Fe_4Rh_2(CO)_{16}B]^-$ is the most stable isomeric form can be attributed to either an energetically preferred ligand arrangement or a metal–metal bonding network for the trans form or both. As we have no geometric information on the ligand arrangement of the cis form, we cannot comment on the first possibility. Heteronuclear diatomic bonds have energies greater than the mean of the homonuclear bond energies.[31] On this basis, the trans isomer, having the greater number of heteronuclear bonds, might be expected to be more stable.

(24) Rath, N. P.; Fehlner, T. P. *J. Am. Chem. Soc.* **1988**, *110*, 5345. Fehlner, T. P.; Czech, P. T.; Fenske, R. F. *Inorg. Chem.* **1990**, *29*, 3103. Khattar, R.; Fehlner, T. P.; Czech, P. T. *New J. Chem.*, submitted for publication.
(25) Bor, G.; Stanghellini, P. L. *J. Chem. Soc., Chem. Commun.* **1979**, 886.
(26) Oxton, I. A.; Powell, D. B.; Farrar, D. H.; Johnson, B. F. G.; Lewis, J.; Nicholls, J. N. *Inorg. Chem.* **1981**, *20*, 4302.
(27) Creighton, J. A.; Pergola, R. D.; Heaton, B. T.; Martinengo, S.; Strona, L.; Willis, D. A. *J. Chem. Soc., Chem. Commun.* **1982**, 864.
(28) Oxton, I. A.; Powell, D. B.; Goudsmit, R. J.; Johnson, B. F. G.; Lewis, J.; Nelson, W. J. H.; Nicholls, J. N.; Rosales, M. J.; Vargas, M. D.; Whitmire, K. H. *Inorg. Chem. Acta* **1982**, *64*, L259.
(29) Stanghellini, P. L.; Cognolato, L.; Bor, G.; Kettle, S. F. A. *J. Cryst. Spectrosc. Res.* **1983**, *13*, 127.
(30) Stanghellini, P. L.; Rossetti, R.; D'Alfonso, G.; Longoni, G. *Inorg. Chem.* **1987**, *26*, 2769.
(31) Porterfield, W. F. *Inorganic Chemistry*; Addison-Wesley: Reading, MA, 1984; p 59.

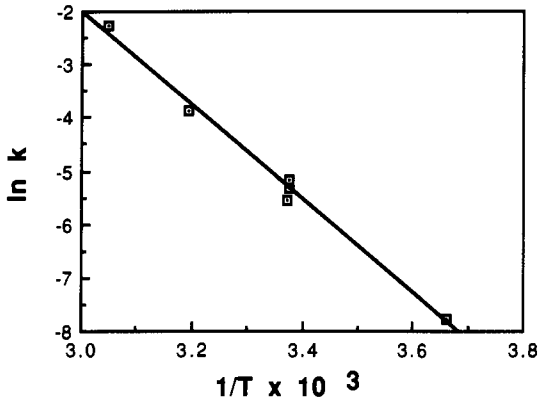

Figure 4. Plot of ln k vs $1/T \times 10^3$ for the isomerization reaction. $y = 24.5 - 8.84x$, $R = 1.00$, $E_a = 17.6$ kcal/mol, and $A = 7.4 \times 10^8$ s^{-1}.

The initial formation of *cis*-$[Fe_4Rh_2(CO)_{16}B]^-$ in the preparative reaction requires that the addition of two rhodium carbonyl fragments to $[HFe_4(CO)_{12}BH]^-$ be fast relative to cluster isomerization, reaction 1. The kinetics of reaction 1 have been in-

$$cis\text{-}[Fe_4Rh_2(CO)_{16}B]^- \rightarrow trans\text{-}[Fe_4Rh_2(CO)_{16}B]^- \quad (1)$$

vestigated under a variety of conditions, and the measured pseudo-first-order rate constants are gathered in Table I. Typical data are shown in Figure 3. These observations serve to limit the number of mechanistic possibilities.

The CO dependence[32] defines the rate law to be that given in (2), and hence, the isomerization is associative in nature, as shown in eq 3. The increased rate on the addition of phosphine confirms

$$\text{rate} = k_2[CO][\text{cluster}] \quad (2)$$

$$cis\text{-}[Fe_4Rh_2(CO)_{16}B]^- + CO \rightarrow trans\text{-}[Fe_4Rh_2(CO)_{16}B]^- + CO \quad (3)$$

the associative nature of the reaction whereas the insensitivity of the rate to added amine suggests that coordination of the ligand takes place at a metal center.

The increased rate in changing solvents from THF to Et_2O is attributed in part to the increased solubility of CO in the latter solvent.[33,34] The insensitivity of rate to the nature of the cation suggests, at maximum, weak ion–ion association. The possible roles of HCl (presumably produced in the reaction of $[HFe_4(CO)_{12}BH]^-$ with $[Rh(CO)_2Cl]_2$) and fortuitous excess $[Rh(CO)_2Cl]_2$ are shown to be negligible by the insensitivity of the rate to added $NaHCO_3$ or $[Rh(CO)_2Cl]_2$, respectively.

The nature of the CO dependence of the rate of isomerization shows, within experimental error, that the contribution of any CO-independent pathway to the overall isomerization is zero. This means that the isomerization rates, measured without deliberately adding CO, must be attributed to the presence of adventitious CO in the reaction system. This is confirmed by the substantial reduction in overall rate with continuous N_2 purge and reflects the high sensitivity of the reaction rate to CO. However, the measurements carried out without a purge were reproducible under similar experimental conditions and the temperature dependence of the apparent first-order rate constants with no purge is illustrated in the Arrhenius plot shown in Figure 4. The magnitudes of the activation energy and Arrhenius A factor (17.6 kcal/mol and 7×10^8 s^{-1}) are reasonable for reaction 3 (see below) but contain systematic errors only some of which are known; viz., the solubility of CO depends on temperature.

Reaction 3 need not be and probably is not a single-step process. One crucial question is whether the facilitating Lewis base enters the coordination sphere of one of the metal atoms of the boride on a time scale the same as or different from that of the isomerization. One can envision two limiting possibilities. In the first, the Lewis base coordinates, isomerization takes place, and the base leaves. In the second, the Lewis base coordinates and becomes indistinguishable (in the case of CO) from the original cluster carbonyl ligands before or during isomerization such that all 17 ligands in the intermediate have equal probability of being lost. In the case of phosphine rather than CO, the question is basically whether the formation of *trans*-$[Fe_4Rh_2(CO)_{15}(PR_3)B]^-$ is or is not competitive with isomerization.

To attack this problem, additional information on the role of phosphine as a promoter of the isomerization reaction was sought by observing both the ^{31}P NMR and ^{11}B NMR spectra from the same sample as a function of time. In this manner, the rate of isomerization could be measured from the time variation of the ^{11}B NMR signal and evidence for intermediates and/or substitution by phosphine could be sought in the ^{31}P NMR spectrum. In the presence of a 3-fold excess of PMe_2Ph, no ^{31}P resonance at all was observed during the course of the isomerization reaction.[35] However, in the presence of a 30-fold excess of phosphine, a broad signal was observed at $\delta \sim -5$ during isomerization. The rate of isomerization increased by approximately a factor of 10 in going from the 3:1 to the 30:1 reaction mixtures, as expected for a first-order dependence on phosphine concentration. Addition of a vast excess of phosphine to the first reaction mixture (initial phosphine to boride ratio of 3) after the isomerization was complete resulted in the production of a broad resonance at δ −28 and weak resonances at δ −5.5 (d, $J_{RhP} = 150$ Hz) and 28.6 (s) in ca. 1 h. A similar experiment on the second reaction mixture resulted in a broad resonance at δ −34 along with weaker signals at δ −5.5 (d, $J_{RhP} = 150$ Hz), 29.0 (s), and 42.0 (s).

These observations can be explained with the following set of reaction steps:

$$cis\text{-}[Fe_4Rh_2(CO)_{16}B]^- + PMe_2Ph \leftrightarrow \{cis\text{-}[Fe_4Rh_2(CO)_{16}B]^-\}\cdot PMe_2Ph \quad (4)$$

$$\{cis\text{-}[Fe_4Rh_2(CO)_{16}B]^-\}\cdot PMe_2Ph \rightarrow trans\text{-}[Fe_4Rh_2(CO)_{16}B]^- + PMe_2Ph \quad (5)$$

$$trans\text{-}[Fe_4Rh_2(CO)_{16}B]^- + PMe_2Ph \leftrightarrow \{trans\text{-}[Fe_4Rh_2(CO)_{16}B]^-\}\cdot PMe_2Ph \quad (6)$$

$$\{trans\text{-}[Fe_4Rh_2(CO)_{16}B]^-\}\cdot PMe_2Ph \rightarrow trans\text{-}[Fe_4Rh_2(CO)_{15}(PMe_2Ph)B^-] + CO \quad (7)$$

Reactions 4 and 5 represent the mechanism for isomerization, and reactions 6 and 7, that for phosphine substitution. The broad resonances with chemical shifts that depend on the phosphine concentration ($\delta \sim -28$, first experiment; δ −5, −34, second experiment) are assigned to an average resonance of free and coordinated phosphines with the condition of rapid exchange on the NMR time scale,[36] hence the justification for steps 4 and 6. The resonance at δ −5.5 (d, $J_{RhP} = 150$ Hz) is assigned to *trans*-$[Fe_4Rh_2(CO)_{15}(PMe_2Ph)B]^-$ with substitution at Rh whereas the resonance at δ 28.6 corresponds to a compound of the same composition but with substitution at Fe. These chemical shifts are characteristic of the metal sites. Hence, we suggest reaction 7.[37] The actual isomerization step 5 almost certainly takes place indirectly via the adduct rather than directly as written in (3) although this is a difficult point to prove. The fact that signals corresponding to $[Fe_4Rh_2(CO)_{15}(PMe_2Ph)B]^-$ with substitution at Rh or Fe were observed only at long times with excess phosphine

(32) See Figure 1 of ref 23.
(33) The solubility of CO in THF is 0.0109 M atm^{-1} at 298 K: Payne, M. W.; Leussing, D. L.; Shore, S. G. *Organometallics* **1991**, *10*, 574.
(34) The solubility of CO in Et_2O is 0.0163 M atm^{-1} at 295 K: Linke, W. F., Ed. *Solubilities of Inorganic and Metal Organic Compounds*, 4th ed.; Van Nostrand: New York, 1958; Vol. 1, p 456.
(35) PMe_2Ph exhibits a sharp ^{31}P resonance at δ −46.1. When some excess $[Rh(CO)_2Cl]_2$ dimer was present, signals at $\delta \sim 0$ corresponding to Rh substitution were observed. The origin of the signals was determined by monitoring the reaction of the dimer with phosphine.
(36) The fact that no signal was observed in the 3:1 reaction is apparently due to insufficient S:N to detect the weak, broad signal.
(37) Evidence for similar adduct formation preceding substitution in a metallaborane cluster has been reported: Housecroft, C. E.; Buhl, M. L.; Long, G. J.; Fehlner, T. P. *J. Am. Chem. Soc.* **1987**, *109*, 3323.

and never before isomerization was complete demonstrates that reaction 7 is much slower than reaction 5. Both of these in turn are slower than the boride–phosphine adduct equilibria (4) and (6). Hence, direct substitution of the cis isomer is not written as a separate set of steps. The fact that substitution is slower than isomerization rules out a mechanism in which the only role of the phosphine is to produce CO, which then serves as the unique promoter of the isomerization. The only other observed resonance not accounted for is that at δ 42. This signal is assigned to $Fe(CO)_4(PMe_2Ph)$ and indicates that some cluster fragmentation occurs in the presence of excess phosphine. This mononuclear species has been observed previously as a product of ferraborane cluster fragmentation by phosphines.[38]

The above data establish that ligand coordination of a soft ligand to the metal centers of $[Fe_4Rh_2(CO)_{16}B]^-$ is an intimate part of the isomerization process. The addition of a Lewis base to a cluster adds two electrons to the skeletal electron count. In metal clusters this may[39] or may not[40] lead to an opening of the cluster framework; however, addition of two additional skeletal electrons will certainly serve to stabilize more open structures. The ligand promotion of the isomerization process must take place via relatively facile coordination of the phosphine, albeit not necessarily weak coordination. Obviously, there are many possible open structures, and early proposals for intermediates in the rearrangement of octahedral frameworks have identified two.[41] The simplest structure, in the sence of satisfying Wade's rules, is the pentagonal-pyramidal intermediate depicted in the mechanism we favored in our communication.[23] Two isomeric arrangements of the metal atoms in the nido structure of the intermediate lead to net isomerization of the original boride cluster. In one, the Fe–Fe network of *cis*-$[Fe_4Rh_2(CO)_{16}B]^-$ is disrupted and the Rh atoms are adjacent but are in apical and basal positions in a pentagonal-pyramidal intermediate. In the other, the Rh–Rh interaction is broken and the Rh atoms are in nonadjacent positions in the intermediate. However, for phosphine at least, formation of the adduct leading to facile isomerization does not lead to equally facile substitution. Thus, there is some doubt as to whether the intermediate depicted as $\{[Fe_4Rh_2(CO)_{16}B]^-\}$L actually needs to achieve the predicted most stable structure for the available number of cluster electron pairs, i.e., a pentagonal pyramid. As we were unable to observe this intermediate spectroscopically, no conclusion is possible at this point.

The decrease in rate on replacing the $Rh(CO)_2$ fragments with Rh(cod) (cod = cyclooctadiene) presents an interesting concluding comment on the mechanism. One might expect the greater steric bulk of cod relative to two CO ligands to promote rather than inhibit the cis to trans isomerization. Although ligand association is not rate determining, a decrease in the overall equilibrium constant for reaction 4 will result in a decrease in the overall isomerization rate, i.e., in the steady-state approximation $k_{exptl} = k_5K_4$. If Lewis base coordination takes place at a rhodium center, then the greater steric bulk of cod vs two CO's could well cause a decrease in the magnitude of K_4, resulting in the 7-fold decrease in k_{exptl} observed in going from $Rh(CO)_2$ to Rh(cod) fragments.

Given the stoichiometric mechanism for isomerization (reactions 4 and 5), the Arrhenius parameters derived from Figure 4 can be used to provide insight into the nature of the intimate mechanism. In spite of the systematic, but unknown, errors present in these parameters (see above), Benson has amply demonstrated that a knowledge of the order of magnitude of the A factor provides information on the qualitative changes in structure occurring on going from reactant to transition state.[42] In principle, the same is true of the activation energy, but in practice, the energetics are less easily treated. The pseudo-first-order rate constant, $k(1st)$, with $A(1st) = 7.4 \times 10^8\ s^{-1}$, can be converted into that for the overall second-order process by using the measured dependence of $k(1st)$ on CO pressure combined with the solubility of CO in THF. This gives $A(2nd) \approx 10^{11.7}\ M^{-1}\ s^{-1}$. From the mechanism we have

$$k(2nd) = k_5K_4[L]/(1 + K_4[L]) \approx k_5K_4[L] \quad (8)$$

The approximation is justified, as no curvature was observed in the plot of $k(1st)$ vs [CO].[23] Hence

$$A(2nd) = A_5A_4/A_{-4} \approx 10^{11.7}\ M^{-1}\ s^{-1} \quad (9)$$

Now A_4/A_{-4} is directly related to the entropy change in the association reaction, and this has been estimated to be $\leq 10^{-4}\ M^{-1}$ for a prototypical reaction.[43] Thus, $A_5 \geq 10^{15.7}\ s^{-1}$, which implies a transition state with a substantially reduced force field in contrast to that observed for a typical organic isomerization, e.g., that of olefins.[42]

A loose transition state is quite consistent with our suggestion that the cluster opens during the isomerization process. For the purpose of the argument, if we assume a pentagonal-pyramidal transition state, then simply counting edges leads to the conclusion that there should be two fewer metal–metal interactions in the transition state than in the initial octahedral boride. The vibrations associated with the metal–metal interactions are of low frequency and contribute significantly to the overall vibrational entropy of the octahedral boride. In the spirit of Benson,[42] we estimate $\nu(MM) \approx 200\ cm^{-1}$, three modes (two bends and one stretch), and $\Delta S \approx 6.6$ eu for each metal–metal interaction. This leads to

$$A_5 = (kT/h)e^{\Delta S/R} = 10^{13.25+\Delta S/4.575} \approx 10^{16}\ s^{-1} \quad (10)$$

Neither the experimental result nor the estimate of A_5 is very precise, but the similarity of the order of magnitudes of observed and estimated A_5 values is consistent with the mechanistic conclusion.

Most theoretical considerations of polyhedral rearrangements conclude that the barriers associated with the isomerization of octahedral clusters should be large.[44] A generalization derived from one study in particular is that large barriers are to be associated with mechanisms involving intermediates having skeletal electron counts different from that of the rearranging cluster.[45] Nearly all these theoretical studies restrict discussion to unimolecular pathways; however, the characterized transition-metal cluster framework isomerizations,[46-49] although rare, suggest that ligand dependence of the rate must be examined. Further, the nature of the ligand dependence cannot be anticipated; i.e., the rearrangement of one metal–main group atom cluster is known to be inhibited by CO.[50] Here we have demonstrated that ligand association is required for isomerization but that the overall isomerization process is much more rapid than net substitution. The transition state for isomerization appears to be one in which the octahedral boride cluster framework has, at minimum, considerably loosened up and, possibly, opened. The fact that rapid, reversible ligand association precedes rate-determining isomeri-

(38) Housecroft, C. E.; Fehlner, T. P. *J. Am. Chem. Soc.* **1986**, *108*, 4867.
(39) Johnson, B. F. G.; Lewis, J.; Nicholls, J. N.; Oxton, I. A.; Raithby, P. R.; Rosales, M. J. *J. Chem. Soc., Chem. Commun.* **1982**, 289.
(40) Vahrenkamp, H.; Wucherer, E. J.; Wolters, D. *Chem. Ber.* **1983**, *116*, 1219.
(41) Hoffmann, R.; Lipscomb, W. N. *Inorg. Chem.* **1963**, *2*, 231.
(42) Benson, S. W. *Thermochemical Kinetics*: Wiley: New York, 1968.
(43) Garabedian, M. E.; Benson, S. W. *J. Am. Chem. Soc.* **1964**, *86*, 176.
(44) Gimarc, B. M.; Ott, J. J. *Inorg. Chem.* **1986**, *25*, 83. Johnson, B. F. G. *J. Chem. Soc., Chem. Commun.* **1986**, 27. Wales, D. J.; Stone, A. J. *Inorg. Chem.* **1987**, *26*, 3845. Roger, A.; Johnson, B. F. G. *Polyhedron* **1988**, *7*, 1107. McKee, M. L. *J. Am. Chem. Soc.* **1988**, *110*, 5317. Wales, D. J.; Mingos, D. M. P. *Inorg. Chem.* **1989**, *28*, 2748.
(45) Wales, D. J.; Mingos, D. M. P.; Zhenyang, L. *Inorg. Chem.* **1989**, *28*, 2754.
(46) Gladfelter, W. L.; Geoffroy, G. L. *Inorg. Chem.* **1980**, *19*, 2579. Geoffroy, G. L. *Acc. Chem. Res.* **1980**, *13*, 469.
(47) Fjare, D. E.; Gladfelter, W. L. *J. Am. Chem. Soc.* **1984**, *106*, 4799.
(48) Adams, R. D.; Wang, S. *Inorg. Chem.* **1985**, *24*, 4447.
(49) Park, J. T.; Shapley, J. R.; Bueno, C.; Ziller, J. W.; Churchill, M. R. *Organometallics* **1988**, *7*, 2307.
(50) Wucherer, E. J.; Tasi, M.; Hansert, B.; Powell, A. K.; Garland, M.-T.; Halet, J.-F.; Saillard, J.-Y.; Vahrenkamp, H. *Inorg. Chem.* **1989**, *28*, 3564.

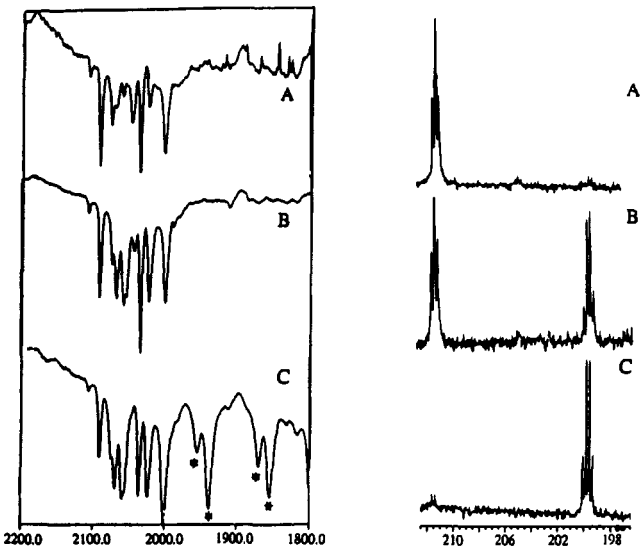

Figure 5. IR (left) and ^{11}B (right) spectra illustrating three stages of the protonation of *trans*-$[Fe_4Rh_2(CO)_{16}B]^-$: (A) hexane extract immediately after protonation; (B) hexane extract 24 h after protonation, showing the formation of $H_2Fe_3Rh_3(CO)_{15}B$ in the ^{11}B NMR spectrum; (C) toluene solution of the final reaction mixture after no further reaction was observed. The starred absorptions in the IR spectrum are due to the solvent.

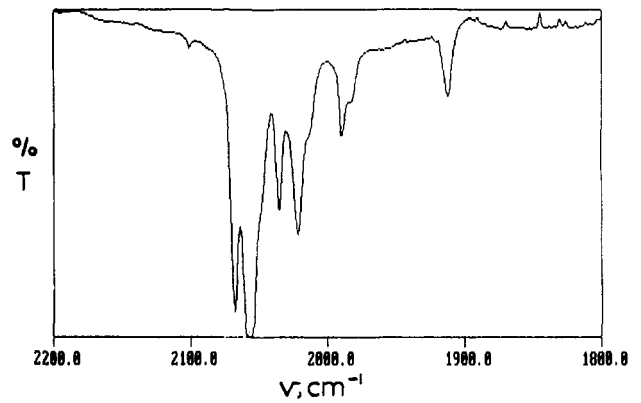

Figure 6. IR spectrum in hexanes of $H_2Fe_3Rh_3(CO)_{15}B$ in the CO stretching region.

zation, as well as the fact that substitution is slow, suggests that the intermediate, {*cis*-$[Fe_4Rh_2(CO)_{16}B]^-$}·PMe_2Ph, has a structure which is not the most stable cluster structure in terms of formal electron count. The importance of high-energy structures in cluster reactivity is a theme we have stressed in earlier work involving hydrocarbyl cluster reactions.[51] Finally, the lability of the cluster framework suggested by the isomerization studies is underlined by the spontaneous conversion of $HFe_4Rh_2(CO)_{16}B$, the product of simple protonation of $[Fe_4Rh_2(CO)_{16}B]^-$ to $H_2Fe_3Rh_3(CO)_{15}B$.

Reactivity: Protonation. Considering the ease with which other anionic metallaboranes such as $[Ru_6(CO)_{17}B]^-$[20] add protons, we expected *trans*-$[Fe_4Rh_2(CO)_{16}B]^-$ to be easily neutralized. In the event, however, only treatment with strong acid under extraction conditions produced a neutral compound, $HFe_4Rh_2(CO)_{16}B$. The ^{11}B NMR shift of this compound is virtually identical to that of the parent anion, suggesting protonation on the metal framework or carbonyl ligands. We were able to observe the proton in the ^1H NMR spectrum only at low temperature. The chemical shift suggests a M–H–M bridging hydrogen, and the lack of coupling suggests bonding to iron rather than rhodium. This neutral cluster is not stable. On standing in solution, the protonated cluster converts to another different neutral compound that gives rise to a quartet in the ^{11}B NMR spectrum to slightly higher field. Analysis of the overall reaction via IR and ^{11}B NMR spectroscopy

(51) Barreto, R. D.; Puga, J.; Fehlner, T. P. *Organometallics* **1990**, *9*, 662.

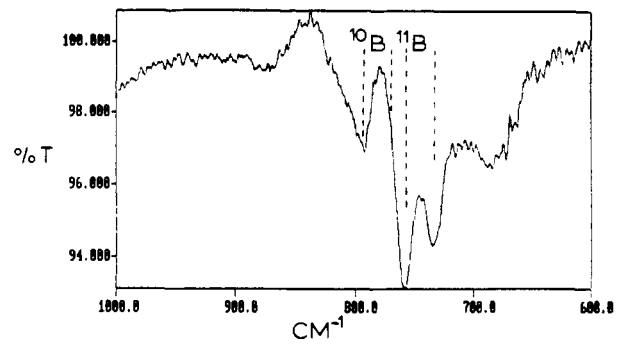

Figure 7. IR difference spectrum of $H_2Fe_3Rh_3(CO)_{15}B$ in Nujol at room temperature.

Table II. Crystallographic Data for $Fe_3Rh_3(CO)_{15}B$

chem formula	space group $Pbc2_1$
$Fe_3Rh_3(CO)_{15}B$	(non-std $PCa2_1$)
a = 14.512 (3) Å	T = 24 °C
b = 19.058 (4) Å	λ = 0.710 73 Å
c = 18.753 (5) Å	ρ_{calcd} = 2.324 g cm^{-3}
V = 5186.8 (22) Å^3	μ = 35.1 cm^{-1}
Z = 8	R^a = 11.09%
fw 907.22	$R_w{}^b$ = 11.35%

$^a R = \sum||F_o| - |F_c||/\sum F_o$. $^b R_w = [w\sum(|F_o| - |F_c|)^2/\sum wF_o^2]^{1/2}$.

shows the complex nature of the reaction. As illustrated in Figure 5, the initial IR spectrum after protonation is considerably more complex than that of the anion, even though the ^{11}B NMR spectrum shows the presence of a single species containing boron. Clearly, additional non-boron-containing metal carbonyls are side products. Likewise, after complete conversion to the new boride, the IR spectrum is more complex than that of the pure neutral boride (Figure 6), but again the ^{11}B NMR spectrum yields a single resonance.

Identification and structural characterization of the final product were difficult and were not completely satisfactory. However what is clear is that it is an extraordinary product for a "simple" protonation reaction, and the following details what we know of it. The mass spectrometric data are consistent with the comparison $H_2Fe_3Rh_3(CO)_{15}B$, and thus the product is a saturated 86-electron cluster, as is $[Fe_4Rh_2(CO)_{16}B]^-$. The low-field quartet with narrow line widths observed in the ^{11}B NMR spectrum (Figure 5) demonstrates the presence of a boron atom in a highly symmetrical electronic environment directly bonded to several metal atoms, three of which are rhodium. With CD_2Cl_2 as the solvent, neither the room-temperature nor the low-temperature ^1H NMR spectra show signals other than those that can be ascribed to impurities or solvent. Hydride signals were observed at low temperature with $(CD_3)_2CO$ as the solvent; however, subsequent observation of the ^{11}B NMR spectrum showed total loss of the signal characteristic of the boride.

The IR spectrum of $H_2Fe_3Rh_3(CO)_{15}B$ in the solid state shows the presence of at least one type of bridging carbonyl. Absorptions that can be associated with interstitial modes (see above) have also been identified (Figure 7). The band with a maximum at 757 cm^{-1} (^{10}B band: observed, 792 cm^{-1}; calculated, 794 cm^{-1}) is clearly associated with an interstitial boron atom. However, the assignment of the band at 735 cm^{-1} with a calculated isotope peak at 771 cm^{-1} is less certain. There is the hint of a shoulder on the 757-cm^{-1} band at ~770 cm^{-1}, but the primary band itself is partially obscured by a weak band from the Nujol matrix at 722 cm^{-1} which has been subtracted from the spectrum shown. Unfortunately, because of this subtraction, the broad bump at 687 cm^{-1} may or may not constitute an additional band. Given the composition of the product, these bands do not provide sufficient information to distinguish between the facial and meridional isomers possible for an octahedral cluster.

The information known on the solid-state structure of the neutral cluster $H_2Fe_3Rh_3(CO)_{15}B$ is summarized in Figure 8, and the crystal data are given in Table II. Spherically shaped metal

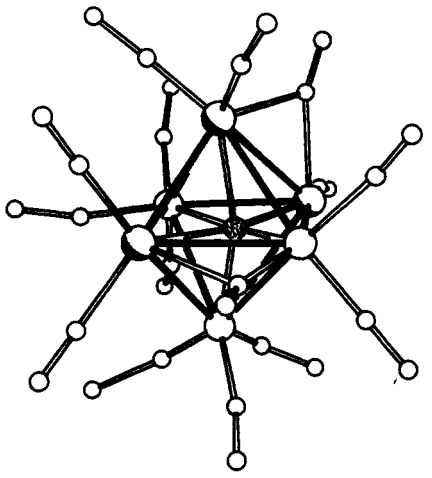

Figure 8. Molecular structure of one of the two crystallographically independent molecules of $H_2Fe_3Rh_3(CO)_{15}B$. In this molecule, the atom positions are ordered, but the identities are not: (shaded, major Rh positions; unshaded, major Fe positions; stipled, B. Atoms are otherwise unlabeled (see text.)

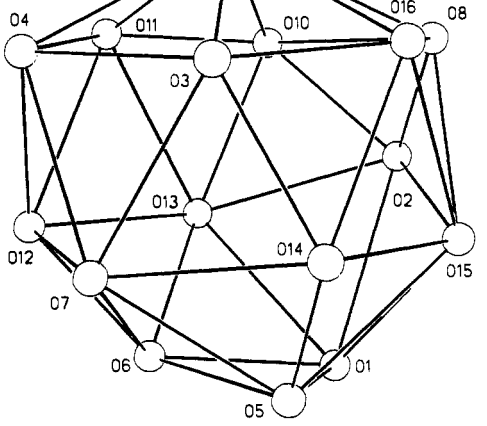

Figure 9. The deltahedron defined by the carbonyl oxygen atoms of *trans*-$[Fe_4Rh_2(CO)_{16}B]^-$.

carbonyl cluster structures frequently crystallize in disordered arrangements, and the spherical shape of $[Fe_4Rh_2(CO)_{16}B]^-$ is illustrated in Figure 9. In the absence of a negative charge, and the associated cation, only weak peripheral, intermolecular forces are present and result in a multitude of nearly isoergic orientations. As is often the case, this circumstance limits the quality of the structural information available for many cluster systems, including this one. As discussed in the Experimental Section, the lack of quality of this structure is not fault of the crystallographic methodology. Thus, although the severe disorder problems do not allow the bond metrics to be obtained, some reliable information is revealed. The results confirm a heavy-atom composition of $Fe_3Rh_3(CO)_{15}B$ and reveal that (for the positionally ordered molecule) the metal atoms are octahedrally arranged and mainly meridionally disposed; there are two μ_2-CO groups, one bridging a Rh–Rh bond and the other an Fe–Rh bond; and a B atom is encapsulated within the cluster. The observed isomer appears to be the meridional isomer, which, again, is the one that contains the maximum number of heteronuclear metal–metal interactions. No attempt has been made to place the hydrogen atoms in this structure, but clearly there is room in the CO ligand envelope for two H ligands.

Integration of the ^{11}B NMR spectra with respect to an external reference suggests that rhodium is the limiting element in the formation of $H_2Fe_3Rh_3(CO)_{15}B$ in that only 70% of the boron of $HFe_4Rh_2(CO)_{16}B$ ends up in the final product. Hence, the overall protonation reaction can be written

$$[Fe_4Rh_2(CO)_{16}B]^- + [H]^+ \rightarrow HFe_4Rh_2(CO)_{16}B + \ldots \quad (11)$$

$$3HFe_4Rh_2(CO)_{16}B \rightarrow 2H_2Fe_3Rh_3(CO)_{15}B + \ldots \quad (12)$$

although the identity of the other product(s) is completely unknown. The stability of $H_2Fe_3Rh_3(CO)_{15}B$ is evidenced by the fact that it was unchanged after heating at 90 °C in toluene for several hours.

Experimental Section

General Procedures. All manipulations were carried out in a high vacuum line or under an inert atmosphere of nitrogen with standard Schlenk techniques.[52] $[Rh(CO)_2Cl]_2$ and $[Rh(cod)Cl]_2$ were purchased from Strem Chemicals and used as received. The compounds $[Rh(CO)PPh_3Cl]_2$[53] and $[Fe_4(CO)_{12}BH_n]^{(3-n)-}$ (n = 0–2)[54,55] were synthesized by literature methods. Solvents used (hexane, diethyl ether, toluene, tetrahydrofuran) were distilled over sodium–benzophenone ketyl. Columns were prepared from silica gel 60, EM Science 70–230 mesh, which was dried in an oven overnight before use.

^{11}B NMR (96.27 MHz) and ^{31}P NMR (121.44 MHz) spectra were recorded on a Nicolet NT-300 spectrometer using $[NBu_4][B_3H_8]$ and D_3PO_4/D_2O as the external references, respectively. ^{11}B shifts are reported with respect to $BF_3{\cdot}OEt_2$ (δ 0), ^{31}P shifts with respect to D_3PO_4 (δ 0), and ^1H shifts with respect to TMS (δ 0). ^{11}B NMR integrals were measured against an external standard of $[NBu_4][B_3H_8]$ in acetone-d_6, which, in turn, was calibrated against a solution of $BH_3{\cdot}THF$ of known concentration. Infrared spectra were recorded on Perkin-Elmer 983 and IBM FT-IR 32 spectrometers. Mass spectra were obtained on a MAT-8430 spectrometer with FAB capabilities.

Reaction of $[M][HFe_4(CO)_{12}BH]$ with $[Rh(CO)_2Cl]_2$ in THF (M = Li, Na, K). The sodium salt of $[HFe_4(CO)_{12}BH]^-$ (50 mg, 0.084 mmol) was dissolved in THF (2 mL), and the mixture was stirred at room temperature. A solution of $[Rh(CO)_2Cl]_2$ (34 mg, 0.087 mmol in 1 mL of THF) was added to the stirred suspension under N_2, which resulted in an immediate color change from reddish brown to dark brown. A ^{11}B NMR spectrum of the reaction mixture ca. 15 min after mixing shows two signals at δ 204.4 (t, $^1J_{RhB}$ = 23.3 Hz, fwhm = 11 Hz) and 211.3 (t, $^1J_{RhB}$ = 25.8 Hz, fwhm = 11 Hz) with intensities in the ratio of ~5:1 (overall conversion 97% by integration of the ^{11}B NMR signals). If the reaction mixture is left stirring over a period of ca. 16 h in the same solvent at room temperature, the species corresponding to δ 204 is completely converted into that corresponding to δ 211. Integration against a standard shows no loss of boron and quantitative conversion. Removal of the solvent, followed by extraction of any excess $[Rh(CO)_2Cl]_2$ with toluene, leaves a blackish brown residue. IR (ν_{CO}, cm^{-1}, THF): 2040 vw, sh; 2013 s, sh; 2008 vs; 1980 w; 1955 w, br. MS: FAB, p^- m/z 889, 1 B. The anionic product is soluble in THF and CH_2Cl_2 but decomposes slowly in the latter solvent on prolonged standing. Alternatively, after complete conversion to the species with δ 211, the crude mixture was stirred with a little excess [PPN]Cl in the same solvent over a period of 0.5 h. Solvent was then removed under vacuum, and the salt was extracted with Et_2O, leaving behind excess [PPN]Cl as a residue. Single crystals of *trans*-$[PPN][Fe_4Rh_2(CO)_{16}B]$ of X-ray quality were obtained from an Et_2O/hexane solution at −40 °C over a period of 3–4 days.

In an attempt to isolate intermediate products, the stoichiometry of the above reaction was varied. For example, the reaction of $[Na][HFe_4(CO)_{12}BH]$ with a $^1/_4$ equiv of $[Rh(CO)_2Cl]_2$ initially provided a ^{11}B NMR spectrum that showed the presence of $[HFe_4(CO)_{12}BH]^-$ (δ 150) and the borides (δ 205 and 211) along with a broad signal at δ 165. After ca. 30 min, the last signal disappeared and only the starting material and final products were observed. The intermediate, which is presumed to be the Fe_4Rh cluster and perhaps to be responsible for the signal at δ 165, could not be isolated.

Reaction of $[Na][Fe_4(CO)_{12}BH_2]$ with $[Rh(cod)Cl]_2$ and $[Rh(CO)(PPh_3)Cl]_2$ in THF. The sodium salt of $[HFe_4(CO)_{12}BH]^-$ (50 mg, 0.084 mmol) in 2 mL THF was heated in a 10-mm NMR tube at 328 K with $[Rh(cod)Cl]_2$ (cod = cyclooctadiene) (55 mg, 0.112 mmol) for 1.5 h. The progress of the reaction was followed by ^{11}B NMR spectroscopy. After 1.5 h, the NMR spectrum shows complete conversion of $[HFe_4(CO)_{12}BH]^-$ to $[Fe_4Rh_2(CO)_{12}(cod)_2B]^-$. The solvent was removed under vacuum and the residue extracted two or three times with 5 mL of toluene, each time to remove excess unreacted $[Rh(cod)Cl]_2$. The re-

(52) Shriver, D. F.; Drezdzon, M. A. *The Manipulation of Air-Sensitive Compounds*, 2nd ed.; Wiley: New York, 1986.
(53) Steele, D. F.; Stephenson, T. A. *J. Chem. Soc., Dalton Trans.* **1972**, 2161.
(54) Housecroft, C. E.; Buhl, M. L.; Long, G. J.; Fehlner, T. P. *J. Am. Chem. Soc.* **1987**, *109*, 3323.
(55) Rath, N. P.; Fehlner, T. P. *J. Am. Chem. Soc.* **1987**, *109*, 5273.

sulting black residue provided the following spectroscopic information. Yield (^{11}B NMR): 90%. IR (ν_{CO}, cm^{-1}, THF): 2070 vw; 2012 s, 1980 w, sh; 1950 w. NMR: ^{11}B (THF, 20 °C) δ 205.3 (t, $^1J_{RhB}$ = 28.2 Hz), 210.8 (t, $^1J_{RhB}$ = 24.4 Hz); ^{1}H (CD_2Cl_2, 20 °C) δ 4.28 (m, 8 H), 2.51 (m, 8 H), 1.87 (m, 8 H). The relative intensity of the δ 205 signal was 1.2 times that of the δ 211 signal and decreased on standing. MS: FAB, inconclusive. The anionic product is soluble in THF and CH_2Cl_2 and slightly soluble in toluene. We were unable to protonate this material under conditions where *trans*-$[Fe_4Rh_2(CO)_{16}B]^-$ could be protonated.

The reaction of $[HFe_4(CO)_{12}BH]^-$ with $[Rh(CO)(PPh_3)Cl]_2$ was carried out in the same fashion except that the temperature was held at 318 K and the reaction was only complete in 2.5 h. Yield (^{11}B NMR): 82%. IR (ν_{CO}, cm^{-1}, THF): 2075 vw; 2018 s, sh; 2012 vs, 1989 w, sh; 1977 w, sh, 1850 vw, br. NMR: ^{11}B (THF, 20 °C) 210.8 (t, $^1J_{RhB}$ = 23.4 Hz); ^{1}H (CD_2Cl_2, 20 °C) δ 7.1 (m), 2.51 (m, 8 H), 1.87 (m, 8 H). No cis isomer (δ 205) was observed during the reaction; however, transient signals at δ 145 and 165 were observed when the reaction was carried out at room temperature. MS: FAB, inconclusive. The anionic product is soluble in THF and CH_2Cl_2.

Isomerization of *cis*-$[Fe_4Rh_2(CO)_{16}B]^-$. The rate of isomerization of [Na][*cis*-$Fe_4Rh_2(CO)_{16}B$] was measured at four different temperatures. For each measurement, 60 mg of $[Na][HFe_4(CO)_{12}BH]$ was reacted with 42 mg of $[Rh(CO)_2Cl]_2$ in THF (1.5 mL) at room temperature to afford a mixture of cis and trans isomers of $[Na][Fe_4Rh_2(CO)_{16}B]$. The reaction mixture was transferred into a 10-mm NMR tube and the solution analyzed by ^{11}B NMR spectroscopy. About 1200 scans were accumulated over a period of 10–15 min for each point in order to obtain a good signal to noise ratio. The integrals of the δ 205 and 211 resonances with respect to the external standard were taken to be equal to the relative concentrations of the cis and trans isomers, respectively.

Plots of ln $[I_{205}/(I_{205} + I_{211})]$, where I_{205} and I_{211} represent the integrals of the δ 205 and 211 resonances, respectively, vs time were linear up to 90% conversion. Points beyond 90% conversion were not considered because of the large error associated with the small δ 205 signal. Note that the sum of I_{205} and I_{211} relative to an external standard was constant over the time period of the measurements. For the measurements at 273 K, the NMR tube containing the sample was placed in an ice–water bath and measurements of concentrations were obtained at 1-h intervals over a period of 12 h. The NMR probe was maintained at 273 K for data collection. For the 296.5 K measurements, the sample was kept in the NMR probe. For measurements at temperatures greater than room temperature, the sample was heated in a thermostatically controlled water bath for appropriate intervals and then quenched in an ice bath before recording the ^{11}B spectrum at room temperature.

A number of variations in reaction conditions were explored, and the results are gathered in Table I. To test the possible involvement of other chemical agents in the reactions, the decay of *cis*-$[Fe_4Rh_2(CO)_{16}B]^-$ was observed as described above with the following modifications. To investigate the role of HCl, presumably produced in the preparative reaction of *cis*-$[Fe_4Rh_2(CO)_{16}B]^-$, an excess of $NaHCO_3$ was added immediately before the kinetic run was begun. To investigate the role of solvent, the THF used in the preparative reaction was removed under vacuum and replaced with an equivalent amount of the desired solvent. The Li, Na, and K salts of $[HFe_4(CO)_{12}BH]^-$, prepared from the reaction of Li_2CO_3, $NaHCO_3$, and K_2CO_3 with $HFe_4(CO)_{12}BH_2$, respectively, yielded the corresponding salts of $[Fe_4Rh_2(CO)_{16}B]^-$. To test the effect of CO, the reaction mixture was purged with a continuous flow of N_2 before the kinetic run. The effect of PMe_2Ph on the reaction rate under purged conditions was measured by adding a known volume of the phosphine during the kinetic run. A further test of the role of CO involved replacing the N_2 atmosphere of the preparative reaction with CO. The rate of the latter reaction was too rapid to be measured by ^{11}B NMR spectroscopy. Hence, a study of the CO concentration dependence of the first-order decay of *cis*-$[Fe_4Rh_2(CO)_{16}B]^-$ was carried out as follows.

Mixtures of CO and N_2 were prepared by admitting a desired pressure of CO into a previously evacuated 2-L glass bulb and backfilling with N_2 to a total pressure of 1 atm. *cis*-$[Fe_4Rh_2(CO)_{16}B]^-$ was then prepared in the normal fashion and the reaction mixture degassed by a few freeze–thaw cycles. The desired CO/N_2 atmosphere was then added, the solution was brought to room temperature, and the composition–time data were obtained as described above. In order to convert partial pressures into CO concentrations in THF, the solubility of CO in THF (0.0109 ± 0.0005 M at 298 K at 1 atm of CO)[23] was used.

Estimates of the error associated with temperature control, integration, and the presence of adventitious CO suggest an error of ±15% in the rate constants. The standard deviation of four measurements at 296.5 K is consistent with these estimates. Calculations carried out using the apparent rate constants showed that corrections for reaction taking place during the NMR measurements were negligible.

In the experiments where both ^{31}P and ^{11}B NMR spectra were measured as a function time, the *cis*-$[Fe_4Rh_2(CO)_{16}B]^-$ complex, prepared as noted above, was further purified before the addition of PMe_2Ph as follows. Immediately after preparation, the THF solvent was removed under vacuum and the *cis*-$[Fe_4Rh_2(CO)_{16}B]^-$ salt was washed repeatedly with hexanes to remove completely any excess $[Rh(CO)_2Cl]_2$. The salt was then redissolved in 2 mL of fresh THF for the subsequent NMR studies. ^{11}B NMR spectroscopy was used to follow the rate of isomerization before and after addition of phosphine whereas ^{31}P NMR spectroscopy was used intermittently to look for the presence of reaction intermediates and to determine the relative speed of CO substitution by phosphine.

Protonation of *trans*-$[Fe_4Rh_2(CO)_{16}B]^-$. To a 100-mL Schlenk flask containing a stirring bar and the sodium salt of *trans*-$[Fe_4Rh_2(CO)_{16}B]^-$ (120 mg, 0.20 mmol) were added 20 mL of hexanes and 5 mL of degassed aqueous HBF_4 solution (48%). Continuous stirring over a period of 30 min resulted in the gradual development of an intense brown color in the hexane layer. The clear hexane solution was decanted, and the extraction process was repeated until the hexane solution was almost colorless. An insoluble residue remained in the flask after the acidification and extraction process were complete. The hexane extract (~350 mL) was concentrated to about 20 mL. The ^{11}B NMR spectrum recorded in hexane showed a single boron resonance at δ 211.6 (t, J_{RhB} = 24.2 Hz, fwhm = 13 Hz) whereas the ^{1}H NMR spectrum recorded in CD_2Cl_2 at −80 °C exhibited a single resonance at δ −17.6 (fwhm = 18 Hz). No signal was observed at 22 °C. IR (hexanes, ν_{CO}, cm^{-1}): 2100 vvw, 2091 s, 2075 w, 2069 w, 2058 vw, 2048 m, 2035 vs, 2023 vvw, 2000 m. Integration of the ^{11}B signals against a standard external $[NBu_4][B_3H_8]$ reference showed that ~22% of the original anion was converted into a neutral boride. Over a period of ~7 days at 0 °C or 2 days at room temperature, the δ 211 signal decayed and a new signal at δ 199.7 (q, J_{RhB} = 24.1 Hz, fwhm = 12 Hz) appeared. Integration against a standard external $[NBu_4][B_3H_8]$ reference showed that the species corresponding to δ 199 accounted for 70% of the original boron in the neutral boride. Monitoring the reaction by IR spectroscopy showed the weak features in the spectrum of the neutral boride (vide infra), viz., 2075, 2069, 2058, and 2023 cm^{-1}, gradually appeared with time, resulting in a complicated spectrum. Column chromatography of the final reaction mixture at −10 °C produced a single brown band on elution with hexanes. The hexane solution was concentrated, and X-ray-quality crystals were obtained after standing at 0 °C. Isolated yield: 15% by weight based on the initial anion. $H_2Fe_3Rh_3(CO)_{15}B$: IR (hexanes, ν_{CO}, cm^{-1}) 2101 vvw, 2068 s, 2058 vs, 2034 m, 2021 m, 2014 sh, 1990 w, 1984 sh, 1912 w, br; IR (KBr, ν_{CO}, cm^{-1}) 2090 sh, 2047 vs, 2010 vs, 1982 s, 1906 m, 1808 w, br. No evidence for other isomers was observed during the reaction or purification. MS: negative-ion FAB, m/z 910 (1 B, −6 CO).

Crystallographic Study. The crystallographic data on $H_2Fe_3Rh_3(CO)_{15}B$ are summarized in Table II. A deep red crystal was mounted on a glass fiber. Preliminary photographic characterization revealed *mmm* Laue symmetry. Systematic absences in the reflection data indicated either the orthorhombic space group *Pbcm* or *Pbc*2_1. Both space groups were thoroughly explored. Although neither resulted in a fully successful structure, the latter noncentrosymmetric alternative was preferred, for reasons discussed below. An empirical correction for absorption was applied to the data. The structure was solved by direct methods.

Expansion of the structure clearly indicated the presence of two independent molecules not related by the crystallographic mirror plane imposed in *Pbcm*. In the noncentrosymmetric alternative, two complete independent molecules compose the asymmetric unit. It is this model that was selected for further refinement. Although both of the independent molecules are highly disordered, the two independent molecules differ in the kind of disorder found. In one molecule, the atom positions are ordered, but the atom identities are not. In the other molecule, both the positions and the identities are scrambled. Only in the less disordered of the two molecules was it possible to obtain any reliable structural information. Figure 8 represents the major atom identities. These identities were obtained by refining an occupancy factor for each atom; a common thermal parameter was assumed. The occupancies were normalized to maintain a 3:3 Fe:Rh ratio. The metal atoms in the more ordered molecule were anisotropically refined.

All calculations used the SHELXTL (version 5.1) library of programs (G. Sheldrick, Nicolet/Siemens, Madison, WI).

Acknowledgment. The support of the National Science Foundation is gratefully acknowledged.

Supplementary Material Available: Tables of crystal data, atom coordinates, selected bond distances and angles, and anisotropic thermal parameters (17 pages); a listing of observed and calculated structure factors for $Rh_3Fe_3(CO)_{15}B$ (15 pages). Ordering information is given on any current masthead page.